This is the accepted manuscript made available via CHORUS. The article has been published as:

Enhancements in laser-generated hot-electron production via focusing cone targets at short pulse and high contrast

D. R. Rusby, P. M. King, A. Pak, N. Lemos, S. Kerr, G. Cochran, I. Pagano, A. Hannasch, H. Quevedo, M. Spinks, M. Donovan, A. Link, A. Kemp, S. C. Wilks, G. J. Williams, M. J.-E. Manuel, Z. Gavin, A. Haid, F. Albert, M. Aufderheide, H. Chen, C. W. Siders, A. Macphee, and A. Mackinnon

Phys. Rev. E **103**, 053207 — Published 14 May 2021

DOI: 10.1103/PhysRevE.103.053207

Enhancements in the Laser Generated Hot-Electron Production Via Focusing Cone Targets at Short Pulse and High Contrast

D. R. Rusby,[1] P. M. King,[1,2] A. Pak,[1] N. Lemos,[1] S. Kerr,[1] G. Cochran,[1] I. Pagano,[2] A. Hannasch,[2] H. Quevedo,[2] M. Spinks,[2] M. Donovan,[2] A. Link,[1] A. Kemp,[1] S. C. Wilks,[1] G. J. Williams,[1] M. J.-E. Manuel,[3] Z. Gavin,[3] A. Haid,[3] F. Albert,[1] M. Aufderheide,[1] H. Chen,[1] C. W. Siders,[1] A. Macphee,[1] and A. Mackinnon[1]

[1]*Lawrence Livermore National Laboratory, Livermore, CA 94550, United States of America*
[2]*Department of Physics, University of Texas at Austin, Austin, TX 78712, United States of America*
[3]*General Atomics, 3550 General Atomics Ave, San Diego, CA 92103, United States of America*
(Dated: April 1, 2021)

We report on the increase in the accelerated electron number and energy using novel compound parabolic concentrator (CPC) targets from a short-pulse (~150 fs) high-intensity (>10^{18} W/cm^2) and high contrast (~10^8) laser-solid interaction. We report on experimental measurements using CPC targets where the hot-electron temperature is enhanced up to ~9× when compared to planar targets. The temperature measured from the CPC target is $\langle T_e \rangle$ = 4.4±1.3 MeV. Using hydrodynamic and particle in cell simulations, we identify the primary source of this temperature enhancement is the intensity increase caused by the CPC geometry that focuses the laser, reducing the focal spot and therefore increasing the intensity of the laser-solid interaction which is also consistent with analytic expectations for the geometrical focusing.

Intense short pulse laser driven production of bright high-energy sources, such as x-rays [1–4], neutrons [5–7] and protons [8], has been shown to be an invaluable tool in the study of high energy density science. However, to address some of the most challenging applications, such as x-ray radiography of high areal density objects for industrial and national security applications [1–3, 9], both the yield and energy of the sources must be increased beyond what has currently been achieved by state-of-the-art high intensity laser systems.

The yield and energy of secondary particles is typically dependent on the production of hot electrons whose distribution is commonly parameterized by $f(E) \propto A\exp(-E/T_e)$. Here A depends on the amount of laser energy that is coupled into a population of highly energetic and high-current electrons (known as hot-electrons), E is the kinetic energy of the hot-electrons and T_e is their temperature. High values of both A and T_e are important for high-energy Bremsstrahlung production; one can optimize the target thickness to achieve the most dose, however in order to create the highest energy x-rays, the highest energy electrons achievable is desirable [10].

When interacting with a solid target, both of these scale with the normalized vector potential of the laser, a_0, [11–16] which is proportional to the incident intensity of the laser, $a_0 \approx 0.85\sqrt{I_{18}\lambda_\mu^2}$, where I_{18} is the intensity in units of 10^{18} W/cm^2 and λ_μ is the wavelength of the laser in microns. To control and/or enhance the yield and energy of secondary sources, much work has gone into research methods to increase A and T_e through the use of pre-formed plasmas[17–19], advanced nanowire[20–23] or focusing plasma mirrors[24]. Targets as or with cone structures can be used to guide and/or confine the laser and plasma [25–28].

While several numerical studies have been performed on high intensity laser-cone interactions [25, 28–31], there have been relatively few experimental studies [26, 27, 32, 33]. The target used in this study, which is of particular interest, is a Compound Parabolic Concentrator (CPC)[34]. CPC targets are unique compared to other iterations of cones, typically straight walled cones or capillaries, as they are specifically designed to focus light into a smaller area, enabling concentration of light and utilization of the energy at the extremities of a focal spot distribution. While CPCs can be applied to larger facilities such as NIF-ARC or LMJ-PETAL [35] where the facility design requires that large F-number optics must be used, they can also be used more generally on smaller laser facilities to enable access to regimes previously inaccessible.

Here we investigate the interaction between a high-intensity laser and the novel CPC target in a regime not previously studied; that of a short pulse (~150 fs) and high contrast (~10^8) where plasma expansion within the cone target is minimal. Previously presented experimental results on CPC targets [34, 36] used much longer pulse durations (10's ps). For shorter laser pulses, the evolution of the plasma over the duration of the pulse is not critical to the interaction between the laser and the sub-critical density plasma ($< 1 \times 10^{21}$ cm^{-3}), whereas for a longer pulse the plasma can fill the CPC. For such long pulses and plasma filling, the hot-electrons are accelerated super-ponderomotively [37, 38]. Therefore, due to our relatively plasma-free cone, under our experimental conditions we are able to operate the CPCs as geometric focusing devices. This allows us to focus the laser light using this micro focusing target and increase the intensity of the laser solid interaction which leads to an enhancement in electron acceleration via the ponderomotive acceleration mechanism [14]. The enhancements in

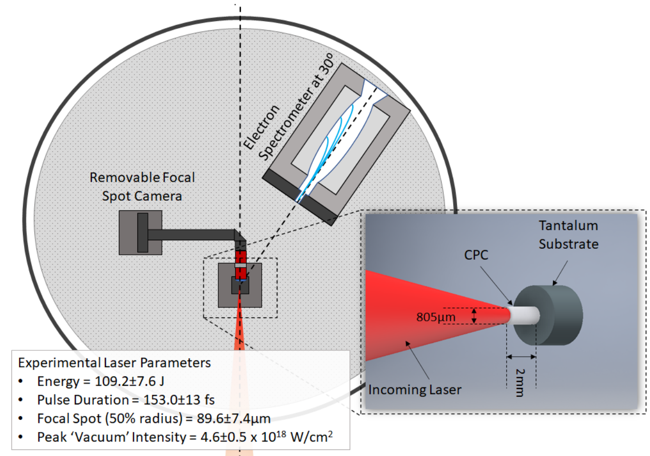

FIG. 1. A top down schematic of the experimental setup showing the target, laser and electron-spectrometer. A 3D drawing of the CPC, Tantalum substrate and the incoming laser is also shown.

the hot-electron temperature that we observe, up to $\sim 9\times$ higher than when using a planar target geometry, are consistent with an analytical analysis of the geometric focusing. We also conclude, due to the enhancements we see in the electron distribution, that CPC targets are ideal candidates as a future target design for many areas of secondary source development where intensity/electron temperature is critical to scaling [10, 39]. Finally, we show that this conclusion is consistent with 2/3D Particle In Cell (PIC) simulations.

The experimental campaign was conducted on the Texas Petawatt (TPW) Laser system at the University of Texas in Austin[40]. The TPW laser is 1.054μm laser that delivered 109.2 ± 7.6 J on target with a pulse duration of 153.0 ± 13 fs during the experiment. We used a F/40 spherical focusing optic where the Rayleigh range is $\approx$14.9 mm, therefore the size of focal spot does not vary over the length of the 2mm long CPC. The focal spot has a 50% enclosed energy at a radius 89.6 ± 7.4 μm and 90% at $291.0 \pm 16.6\mu$m. An example focal spot is shown in Figure 2 a) on a logarithmic intensity scale. All values and uncertainties given are averages and standard deviations from the experimental shots. The average peak intensity is $4.6\pm0.5\times10^{18}$W/cm^2, an a_0 of 3.9 ± 0.4. The power contrast of the TPW laser system[41] is $\sim 5\times10^8$ and $\sim 10^7$ at 200 ps and 20 ps respectively. There is also an intrinsic pointing instability introduced from the laser. From recording the centers of 50 focal spots, this instability is 62.3 μm and 75.3 μm in the horizontal and vertical directions respectively.

The original description of CPCs are given by H. Hinterberger and R. Winston in 1966 [42]. The inner surface of the CPC is a rotated parabola that is tilted about a point below the tip. Light that enter the opening aperture of the CPC within the tilted angle are transported to the tip of the CPC. The CPC targets used in this study leveraged novel fabrication methods utilizing two-photon-polymerization (2PP). This production technique provided the means to produce many nearly-identical CPCs with a tip diameter of 65 μm, which is smaller than the focal spot, and an opening aperture of 805 μm. The 2PP-printed CPCs were then attached to a 2 mm tantalum disc. The CPC here is specifically designed for the final F/40 focusing optic. The focal spot and CPC dimensions are shown in Figure 2 a) and b) respectively. The focal spot is much larger than the tip of the CPC, hence the CPC is reducing the focal spot size. Tantalum discs of the same dimensions are used as a baseline, and will henceforth be referred to as planar targets. Previously, the CPCs were produced via a diamond-turned mandrel [34].

To measure the escaping electron energy distribution, a electron spectrometer[43, 44] was deployed at 30 degrees with respect the laser axis. The signals are recorded on Fuji MS Image Plates for which extensive calibration material exist [45–48].

Multiple laser shots were performed on both planar and CPC targets at maximum intensity. Figure 2 c), shows a sample of electron spectra for the planar and CPC targets from multiple shots. 7 shots were preformed on the planar 2mm tantalum targets at highest intensity. The average electron temperature from these shots was $\langle T_{e(planar)} \rangle = 0.51\pm0.25$ MeV. 10 shots were performed on the CPC target at highest intensity. The average electron temperature from the CPCs is $\sim 9\times$ greater than the planar targets $\langle T_{e(CPC)} \rangle$ $=4.4\pm1.3$ MeV. The uncertainty for both cases is given by the sample standard deviation. The calculated incident intensity as function of measured electron temperature is shown in Figure 2 d). As shown, additional measurements with lower intensities were taken which is achieved by increasing the pulse duration up to 5 ps on the CPCs and 2 ps planar targets. On-shot measurements of the pulse duration for pulses longer than 500 fs could not be made, therefore the uncertainty becomes ±1 ps.

For high intensity laser-solid interactions with steep density profiles, the relationship between the intensity and the electron temperature can be described using the ponderomotive scaling, where $T_{pond} = m_e c^2 \left(\sqrt{1 + a_0^2/2} - 1 \right)$ [14]. For the peak intensity of 4.6×10^{18} W/cm^2 the resulting ponderomotive temperature is $\sim$0.55 MeV which is in close agreement with the planar targets. In Figure 2 d), the electron temperature recorded from the CPCs, at peak intensity and with the longer pulse durations, is fitted well to a ponderomotive scaling which is increased by a factor of 9. Hence we can initially assume that the density profile within the CPC for all pulse durations is steep.

The focusing geometry of the CPC target and the utilisation of laser energy that exists in the outer region of

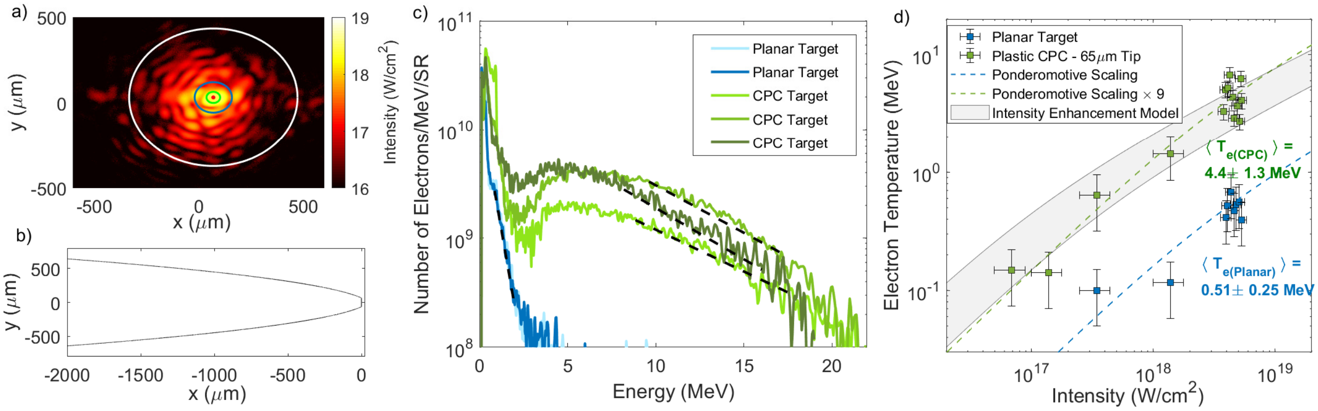

FIG. 2. a) A sample focal spot on a logarithmic intensity scale. The outer white line represents the acceptance aperture of the CPC and the inner green circle is the tip of the CPC. The Blue circle represents the radius at which 50% of the energy is enclosed. b) The geometry of the CPC used on the experimental campaign. The opening aperture is 805 μm and the tip is 65μm. c) A sample of the electron spectra retrieved from different individual shots using the electron spectrometer on CPCs (Green) or Planar (Blue) Targets. The dashed line represent the regions where the electron temperature is fitted. There is a clear enhancement in electron spectra when using CPC targets. d) The hot-electron temperature from planar and CPC targets plotted against the incident laser intensity. Lower intensity points correspond to the pulse duration scan that was performed. Both planar and CPC targets follow a ponderomotive scaling, with the CPCs having a factor of 9 enhancement. The shaded region represents the enhanced electron temperature using the ponderomotive scaling and a purely geometric focusing that increases intensity.

the focal distribution is hypothesized as the source of this enhancement of electron temperatures. Analytically, this can be considered through geometric focusing to estimate the intensity at the tip and using the ponderomotive scaling to calculate the electron temperature.

For the planar target, we assume that only regions of the focal spot where the intensity is greater than 1×10^{18} W/cm^2 is important to the generation of hot-electrons as this is the intensity at which the motion of the electron within the electric field becomes relativistic. This corresponds to approximately a region with a radius, $R_{FocalSpot}$, of 106$\pm$17 μm and 42$\pm$3% of the total energy, $E_{>I18}$. The geometry of the CPCs will affect both of these values. The opening diameter of the CPC captures upto 92$\pm$1% of the laser energy, E_{CPC}, as shown in Figure 2 a). We then assume that the geometry of the CPC transports all of the captured laser energy to the 32.5 μm tip, R_{Tip}. Under these assumptions, the CPC is behaving as initially designed; increasing the energy and decreasing the area of the interaction. The model presented here can be used to predict the intensity for different CPC geometries and lasers. An important consideration is the previously mentioned pointing instability of the laser. If the tip of the CPC is reduced, the opening aperture is also reduce. As well as not capturing as much of the laser, the affects of pointing instability will decrease the effectiveness of the CPC.

The total intensity enhancement can therefore be estimated by taking the ratios of the previously discussed variables; $I_{enhance} = (R^2_{FocalSpot}/R^2_{Tip}) \times (E_{CPC}/E_{>I18})$. This is similar to the methodology presented by Wilson et al[24] for the enhancement provided by ellipsoidal plasma mirrors. The enhancement of this optic also depends on reflectivity of the plasma mirror under high intensity conditions. For the CPC at peak intensity, the majority of reflection are at glancing angles and at intensity between 10^{12-15} W/cm^2. Using HYDRA simulations [49] of the laser pedestal that interacts with the CPC walls prior to the main pulse, the temperature of the walls is calculated to be $\approx$3 eV and with a scale length of $\approx 0.3\mu$m. Under these conditions, particularly with the 150 fs laser pulse where the scale length isn't expected to grow vastly over the peak laser duration, we expect the reflectivity to be high.

For the average focal spot, laser energy and pulse duration, the model yields an intensity increase of $\sim\times36$. Using the ponderomotive scaling, this would yield a electron temperature of $\sim$4.9 MeV. This calculation is performed for all record focal spots, as well as variations in the pulse duration and laser energy to provide upper and lower values for the estimated temperature enhancement; this is shown as a shaded region in Figure 2 d). This simple model does not include field enhancements up to a factor of 4 that will occur due to constructive interference of the focused laser at the tip which can lead to further enhancements in the hot-electron temperature [50], however, PIC simulations in the following section will take this into account.

Using numerical simulations, hydrodynamic and PIC, we can consider the role that interference and plasma have on the accelerated electron population and confirm our intensity enhancement argument. Firstly we con-

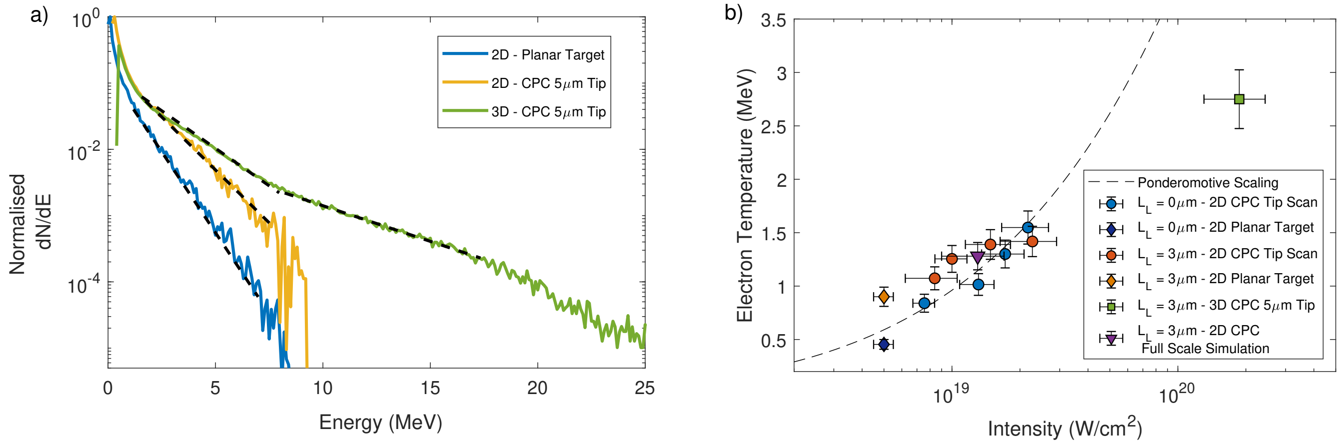

FIG. 3. a) Hot electron spectra from a 2D planar, 2D CPC and 3D CPC PIC simulation. Dashed Line represent temperature fits to spectra. b) The intensity and hot electron temperature extracted from the 2D and 3D PIC simulations. The intensity enhancements due to the focusing nature of the CPCs directly effects temperature of the accelerated electrons.

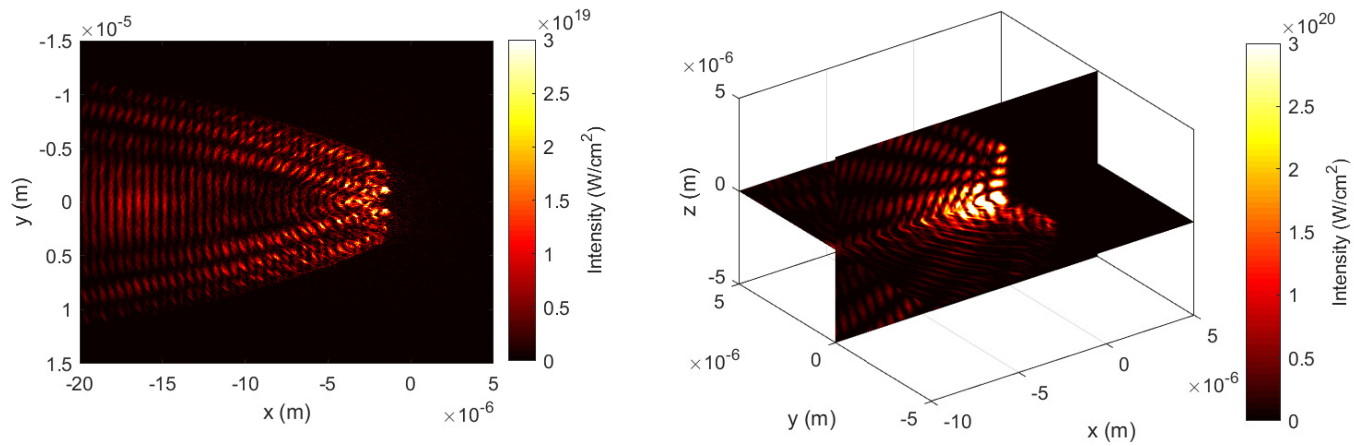

FIG. 4. c) and d) show intensity profiles from the 2D and 3D PIC simulations respectively for the same tip size (5 μm). The intensity achieved in the 3D simulation is greater than that achieved in the 2D simulation due to the extra focusing dimension.

duct HYDRA simulations [49] to estimate the plasma growth prior to the peak laser arrival within the CPC. These simulations use the measured focal spot and contrast/prepulse of the laser, as well as the geometry of the CPC, to accurately recreate the focusing condition prior to the pulse. A small plasma develops at the tip of the CPC that follows a double decaying exponential that can be approximated as $n(x) = n_s e^{-x/L_S} + n_c e^{-x/L_L}$, where, n_s and n_c the solid and critical density respectively and L_S and L_L are the 'short' and 'long' scale length respectively where L_S =0.5μm and L_L =3μm.

The PIC simulations are conducted using EPOCH [51]. In order to investigate the intensity enhancement and its influence on the hot-electron generation, multiple 2D and 3D simulations are conducted with varying tips sizes. Whilst 2D simulations are easier to perform, it is important to simulate the CPC geometry in 3D as there will be an additional focusing dimension. In 2D the CPC more closely resembles a wedge rather than a cone. Despite this, 2D simulation will provide some focusing and multiple simulations can be performed to demonstrate the focusing nature of the CPCs. Following the analytical approach earlier, it is expected that smaller tips will yield higher intensities and therefore hotter electron temperatures. Due to the spatial size of the CPCs, the majority are conducted at a reduced scale of ∼6 in order to make them less computationally expensive. However, a single 2D PIC simulation was conducted at full experimental scale in order to validate the spatial reduction approach and to take into account the effect of large focal spot on electron acceleration [36].

For the reduced sized 2D simulations, the box size is 105×120 μm with cell sizes of 40 nm and 40 particles per cell whereas the 3D simulation has a reduced spatial resolution (62.5nm) and overall box size (90×44×44μm) in order to make the simulation computationally viable.

The spatial profile of the beam is a double Gaussian with full width half maximums of 20μm and 65μm with a intensity ratio of 1:0.17; determined from intensity profiles of the experimentally measured focal spot. The peak input laser intensity is 5×10^{18}W/cm^2 with a pulse duration of 150 fs full width half maximum and a wavelength of 1.054μm. The soild ion and electron densities are set to 50 $\times$ critical density and the initial electron temperature is set to 50 eV.

The electron spectra from 3 simulations are shown in Figure 3 a) for a 2D planar target, 2D CPC and 3D CPC target where the CPC simulations in 2D and 3D have a tip size of 5μm. The CPCs have a clear increase in the observed temperature of the electrons when compared to the planar target, with the 3D simulations yielding the highest energy electrons, a temperature of 2.75$\pm$0.4 MeV. This is to be expected as the 3D simulation has the greatest intensity enhancement due to the additional focusing dimension. Intensity maps of the two CPC simulations at roughly peak intensity are shown in Figure 4 c) and d). The peak and average intensity at the tip in the 3D simulation are $\approx4\times10^{20}$ W/cm^2 and $\approx7.6\times10^{20}$ W/cm^2 respectively. The electron temperature for this intensity is below the ponderomotive scaling, as shown in figure 3 b). This is likely due to the fact that in order to simulate the system in 3D, the cone (as well as the laser parameters) had to be scaled down in size, thus diluting the intensification effect and reducing the transverse stochastic acceleration effects observed with large focal spot [36].

The size of the CPC tip is varied and simulated in 2D to demonstrate the effect of focusing. The tips have diameters of 5 μm, 10 μm, 15 μm and 25 μm. Each case is conducted with and without $L_L = 3$ μm. The case without a longer scale length represents the idealized case where geometric focusing should be the dominant effect. The intensity of the interaction is found by measuring the peak and average intensity at the approximate time that the peak laser intensity would be interacting with the surface of the target. The hot-electron temperature and intensity for the 4 CPC targets and planar target for the two different L_L are shown in Figure 3 b). As the tip size is reduced, the focused intensity at the tip and extracted electron temperature increases which closely follows the ponderomotive scaling. For both scale length cases, the CPCs have higher electron temperatures than the planar targets. However, the longer scale length planar target has a 3 times higher electron temperature compared to when there is no longer preplasma, and hence, the enhancement from planar to CPC is reduced for longer scale lengths. Whilst the scale length is still relatively short, as suggested by the HYDRA simulation for the condition on the experiment, the dominant enhancement process is still focusing. For much longer scale lengths ($> 2L_L$), the interaction will become more similar to that shown in simulations performed by Kemp et al [38] and experimental and simulations results by William et al[36]. In these cases, the acceleration is primarily due to bulk plasma interactions and direct laser acceleration.

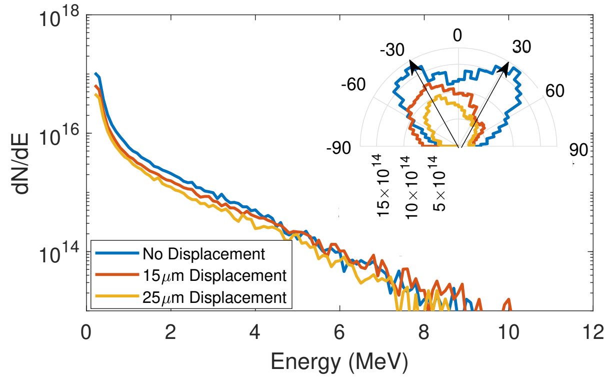

FIG. 5. Electron spectra produced when the laser is pointed in the middle and with 15μm and 25μm displacement in a 2D PIC simulation. Inset shows the change in angular distribution of electrons with energies greater than 1 MeV. The arrows represent the directions of the experimental detection of the electron spectrum.

The full scale 2D simulation is conducted with a tip size of 65μm with a L_L equal to 3μm. The simulation box is 500$\times$390μm with the same spatial resolution and particles per cell as before. The temperature of the electrons were 1.28 MeV and the peak and average intensity are 1.1×10^{19}W/cm^2 and 8.8×10^{18}W/cm^2 respectively. This data is similar to that of the the reduced size data shown in Figure 3 a), hence we can ensure the approach of the reduced sized simulations are valid.

To understand the sensitivity of CPC focusing and hot-electron generation to experimental pointing fluctuations, additional 2D simulations were conducted. Experimentally, the pointing instability is approximately a spot width, therefore simulations are conduction with displacements of 15 μm and 25 μm into the 5 μm tip simulation. The hot-electron spectra and angular distributions of greater than 1 MeV are shown in Figure 5. Whilst the electron temperature of the entire distribution has changed very little, there is a significant change in the angular distribution. This change in angular distribution is primarily caused by the laser reflecting off wall of the CPC towards the opposite corner of the tip. This caused the interaction to be more oblique than the case where the laser has no displacement. Experimentally, the electron spectrum is measured at a single point at 30° with respect to the laser axis, in the simulations this refers to either -30° and 30°, highlighted by the arrows in Figure 5 inset. From the three simulations, the average hot-electron temperature at the angles of interest is $\langle T_e \rangle = 1.30\pm0.20$ MeV. The number of electrons at these angles also vary by a factor of $\sim$3. The changes in the simulated numbers of electrons, angular distribution and temperature induced by mispointing could be a source of the shot to shot variations observed in the experimentally measured electrons we observe on our spectrometer, as shown in Figure 2 a).

We have experimentally demonstrated the capability of focusing cylindrical parabolic concentrator targets that have significantly increased the production of MeV electrons compared to interactions with planar targets.

Due to the high contrast and short pulse nature of the Texas laser pulse, we find from HYDRA simulations that the electron density gradient is steep at the target surface and thus we can assume that ponderomotive acceleration primary mechanism of acceleration. Therefore the increase in the intensity due to the focusing of the CPC directly causes increases in the temperature of the electrons. The $\sim 9\times$ temperature enhancement observed between the planar and CPC target here are consistent with an analytical analysis of geometric enhancement of the laser intensity at the tip of the CPC. This enhancement is higher than that observed by Macphee et al [34] and Williams et al [36]. This primarily due to the laser conditions that form a plasma on the planar target surface and within the CPC, changing the electron acceleration mechanism. This interpretation is supported with detailed 2D and 3D PIC simulations of the laser plasma interaction which were largely consistent with enhanced focusing at the cone tip. The increase in the generation of hot-electrons, both number and temperature, is significant as this is a critical requirement for the development of bright secondary x-ray sources for radiography and other applications. A future publication containing full analysis of the enhancements of the x-ray generation measured on this experiment are to be published at a later date. [reference: private communication: P. M. King et al].

The authors would like to thank the facility staff at the Texas Petawatt Facility for their help conducting the experiment. This work was supported by DOE Office of Science, Fusion Energy Sciences under Contract No. DE-SC0019167 the LaserNetUS initiative at Texas PetaWatt.

This work was performed under the auspices of the U.S. Department of Energy by Lawrence Livermore National Laboratory under Contract DE-AC52-07NA27344 and funded by the LLNL LDRD program under tracking code 19-SI-002 and NNSA contract DE-NA0001808 for target support from General Atomic. Release under the IM:LLNL-JRNL-813462.

[1] C. Courtois, R. Edwards, A. Compant La Fontaine, C. Aedy, M. Barbotin, S. Bazzoli, L. Biddle, D. Brebion, J. L. Bourgade, D. Drew, M. Fox, M. Gardner, J. Gazave, J. M. Lagrange, O. Landoas, L. Le Dain, E. Lefebvre, D. Mastrosimone, N. Pichoff, G. Pien, M. Ramsay, A. Simons, N. Sircombe, C. Stoeckl, and K. Thorp, Physics of Plasmas **18**, 023101 (2011).

[2] C. M. Brenner, S. R. Mirfayzi, D. R. Rusby, C. Armstrong, A. Alejo, L. A. Wilson, R. Clarke, H. Ahmed, N. M. Butler, D. Haddock, A. Higginson, A. McClymont, C. Murphy, M. Notley, P. Oliver, R. Allott, C. Hernandez-Gomez, S. Kar, P. McKenna, and D. Neely, Plasma Physics and Controlled Fusion **58**, 10.1088/0741-3335/58/1/014039 (2015).

[3] D. R. Rusby, C. M. Brenner, C. Armstrong, L. A. Wilson, R. Clarke, A. Alejo, H. Ahmed, N. M. H. Butler, D. Haddock, A. Higginson, A. McClymont, S. R. Mirfayzi, C. Murphy, M. Notley, P. Oliver, R. Allott, C. Hernandez-Gomez, S. Kar, P. McKenna, and D. Neely, in *Proceedings of SPIE - The International Society for Optical Engineering*, Vol. 9992, edited by K. L. Lewis and R. C. Hollins (2016) p. 99920E.

[4] H. Sawada, C. Salinas, F. N. Beg, H. Chen, A. J. Link, H. S. McLean, P. K. Patel, Y. Ping, and J. Williams, Plasma Physics and Controlled Fusion 10.1088/1361-6587/ab8413 (2020).

[5] N. Guler, P. Volegov, A. Favalli, F. E. Merrill, K. Falk, D. Jung, J. L. Tybo, C. H. Wilde, S. Croft, C. Danly, O. Deppert, M. Devlin, J. Fernandez, D. C. Gautier, M. Geissel, R. Haight, C. E. Hamilton, B. M. Hegelich, D. Henzlova, R. P. Johnson, G. Schaumann, K. Schoenberg, M. Schollmeier, T. Shimada, M. T. Swinhoe, T. Taddeucci, S. A. Wender, G. A. Wurden, and M. Roth, Journal of Applied Physics **120**, 10.1063/1.4964248 (2016).

[6] S. R. Mirfayzi, H. Ahmed, D. Doria, A. Alejo, S. Ansell, R. J. Clarke, B. Gonzales, P. Hadjisolomou, R. Heathcote, T. Hodge, P. Martin, D. Raspino, E. Schooneveld, A. Yogo, P. Mckenna, and N. J. Rhodes, , 1 (2020).

[7] I. Pomerantz, E. McCary, A. R. Meadows, A. Arefiev, A. C. Bernstein, C. Chester, J. Cortez, M. E. Donovan, G. Dyer, E. W. Gaul, D. Hamilton, D. Kuk, A. C. Lestrade, C. Wang, T. Ditmire, and B. M. Hegelich, Physical Review Letters **113**, 1 (2014).

[8] H. Daido, M. Nishiuchi, and A. S. Pirozhkov, Reports on Progress in Physics **75**, 10.1088/0034-4885/75/5/056401 (2012).

[9] C. Jones, C. Brenner, C. Stitt, C. Armstrong, D. Rusby, S. Mirfayzi, L. Wilson, A. Alejo, H. Ahmed, R. Allott, N. Butler, R. Clarke, D. Haddock, C. Hernandez-Gomez, A. Higginson, C. Murphy, M. Notley, C. Paraskevoulakos, J. Jowsey, P. McKenna, D. Neely, S. Kar, and T. Scott, Journal of Hazardous Materials **318**, 10.1016/j.jhazmat.2016.07.057 (2016).

[10] A. Compant La Fontaine, Journal of Physics D: Applied Physics **47**, 10.1088/0022-3727/47/32/325201 (2014).

[11] J. R. Davies, Plasma Physics and Controlled Fusion **51**, 10.1088/0741-3335/51/1/014006 (2009).

[12] R. J. Gray, R. Wilson, M. King, S. D. R. Williamson, R. J. Dance, C. Armstrong, C. Brabetz, F. Wagner, B. Zielbauer, V. Bagnoud, D. Neely, and P. Mckenna, New J. Phys **20** (2018).

[13] Y. Ping, R. Shepherd, B. F. Lasinski, M. Tabak, H. Chen, H. K. Chung, K. B. Fournier, S. B. Hansen, A. Kemp, D. A. Liedahl, K. Widmann, S. C. Wilks, W. Rozmus, and M. Sherlock, Physical Review Letters **100**, 6 (2008).

[14] S. C. Wilks and W. L. Kruer, IEEE Journal of Quantum Electronics **33**, 1954 (1997).

[15] F. N. Beg, A. R. Bell, A. E. Dangor, C. N. Danson, A. P.

Fews, M. E. Glinsky, B. A. Hammel, P. Lee, P. A. Norreys, and M. Tatarakis, Physics of Plasmas **4**, 447 (1997).
[16] M. G. Haines, M. S. Wei, F. N. Beg, and R. B. Stephens, Physical Review Letters **102**, 1 (2009).
[17] O. Culfa, G. J. Tallents, A. K. Rossall, E. Wagenaars, C. P. Ridgers, C. D. Murphy, R. J. Dance, R. J. Gray, P. McKenna, C. D. Brown, S. F. James, D. J. Hoarty, N. Booth, A. P. Robinson, K. L. Lancaster, S. A. Pikuz, A. Y. Faenov, T. Kampfer, K. S. Schulze, I. Uschmann, and N. C. Woolsey, Physical Review E **93**, 1 (2016).
[18] C. Courtois, A. Compant La Fontaine, O. Landoas, G. Lidove, V. Méot, P. Morel, R. Nuter, E. Lefebvre, A. Boscheron, J. Grenier, M. M. Aléonard, M. Gerbaux, F. Gobet, F. Hannachi, G. Malka, J. N. Scheurer, and M. Tarisien, Physics of Plasmas **16**, 013105 (2009).
[19] M. I. K. Santala, M. Zepf, I. Watts, F. N. Beg, E. Clark, M. Tatarakis, K. Krushelnick, A. E. Dangor, T. McCanny, I. Spencer, R. P. Singhal, K. W. D. Ledingham, S. C. Wilks, A. C. Machacek, J. S. Wark, R. Allott, R. J. Clarke, and P. A. Norreys, Physical Review Letters **84**, 1459 (2000).
[20] S. Jiang, A. G. Krygier, D. W. Schumacher, K. U. Akli, and R. R. Freeman, European Physical Journal D **68**, 10.1140/epjd/e2014-50339-4 (2014).
[21] S. Jiang, A. G. Krygier, D. W. Schumacher, K. U. Akli, and R. R. Freeman, Physical Review E - Statistical, Nonlinear, and Soft Matter Physics **89**, 1 (2014), arXiv:1310.3283.
[22] S. Jiang, L. L. Ji, H. Audesirk, K. M. George, J. Snyder, A. Krygier, P. Poole, C. Willis, R. Daskalova, E. Chowdhury, N. S. Lewis, D. W. Schumacher, A. Pukhov, R. R. Freeman, and K. U. Akli, Physical Review Letters **116**, 1 (2016).
[23] T. Ebert, N. W. Neumann, L. N. K. Döhl, J. Jarrett, C. Baird, R. Heathcote, M. Hesse, A. Hughes, P. Mckenna, D. Neely, D. Rusby, G. Schaumann, C. Spindloe, A. Tebartz, N. Woolsey, and M. Roth, **043106**, 1 (2020).
[24] R. Wilson, M. King, R. J. Gray, D. C. Carroll, R. J. Dance, C. Armstrong, S. J. Hawkes, R. J. Clarke, D. J. Robertson, D. Neely, and P. McKenna, Physics of Plasmas **23**, 10.1063/1.4943200 (2016).
[25] Y. Sentoku, K. Mima, H. Ruhl, Y. Toyama, R. Kodama, and T. E. Cowan, Physics of Plasmas **11**, 3083 (2004).
[26] K. A. Tanaka, R. Kodama, K. Mima, Y. Kitagawa, H. Fujita, N. Miyanaga, K. Nagai, T. Norimatsu, T. Sato, Y. Sentoku, K. Shigemori, A. Sunahara, T. Shozaki, M. Tanpo, S. Tohyama, T. Yabuuchi, J. Zheng, T. Yamanaka, P. A. Norreys, R. Evanse, M. Zepf, K. Krushelnic, A. Dangor, R. Stephens, S. Hatchett, M. Tabak, and R. Turner, Physics of Plasmas **10**, 1925 (2003).
[27] S. A. Gaillard, T. Kluge, K. A. Flippo, M. Bussmann, B. Gall, T. Lockard, M. Geissel, D. T. Offermann, M. Schollmeier, Y. Sentoku, and T. E. Cowan, Physics of Plasmas **18**, 056710 (2011).
[28] T. Kluge, S. A. Gaillard, K. A. Flippo, T. Burris-Mog, W. Enghardt, B. Gall, M. Geissel, A. Helm, S. D. Kraft, T. Lockard, J. Metzkes, D. T. Offermann, M. Schollmeier, U. Schramm, K. Zeil, M. Bussmann, and T. E. Cowan, New Journal of Physics **14**, 023038 (2012).
[29] S. Yang, W. Zhou, J. Jiao, Z. Zhang, L. Cao, Y. Gu, and B. Zhang, Physics of Plasmas **24**, 10.1063/1.4977905 (2017).
[30] L. X. Hu, T. P. Yu, F. Q. Shao, D. B. Zou, and Y. Yin, Physics of Plasmas **22**, 10.1063/1.4913984 (2015).
[31] R. Kodama, K. Mima, K. A. Tanaka, Y. Kitagawa, H. Fujita, K. Takahashi, A. Sunahara, K. Fujita, H. Habara, T. Jitsuno, Y. Sentoku, T. Matsushita, T. Miyakoshi, N. Miyanaga, T. Norimatsu, H. Setoguchi, T. Sonomoto, M. Tanpo, Y. Toyama, and T. Yamanaka, Physics of Plasmas **8**, 2268 (2001).
[32] N. Renard-Le Galloudec, E. D'Humières, B. I. Cho, J. Osterholz, Y. Sentoku, and T. Ditmire, Physical Review Letters **102**, 205003 (2009).
[33] A. G. MacPhee, L. Divol, A. J. Kemp, K. U. Akli, F. N. Beg, C. D. Chen, H. Chen, D. S. Hey, R. J. Fedosejevs, R. R. Freeman, M. Henesian, M. H. Key, S. Le Pape, A. Link, T. Ma, A. J. Mackinnon, V. M. Ovchinnikov, P. K. Patel, T. W. Phillips, R. B. Stephens, M. Tabak, R. Town, Y. Y. Tsui, L. D. Van Woerkom, M. S. Wei, and S. C. Wilks, Physical Review Letters **104**, 055002 (2010).
[34] A. G. MacPhee, D. Alessi, H. Chen, G. Cochran, M. R. Hermann, D. H. Kalantar, A. J. Kemp, S. M. Kerr, A. J. Link, T. Ma, A. J. Mackinnon, D. A. Mariscal, D. Schlossberg, R. Tommasini, S. Vonhof, C. C. Widmayer, S. C. Wilks, G. Jackson Williams, W. H. Williams, and K. Youngblood, Optica **7**, 129 (2020).
[35] A. Casner, T. Caillaud, S. Darbon, A. Duval, I. Thfouin, J. P. Jadaud, J. P. LeBreton, C. Reverdin, B. Rosse, R. Rosch, N. Blanchot, B. Villette, R. Wrobel, and J. L. Miquel, High Energy Density Physics **17**, 2 (2015).
[36] G. J. Williams, A. Link, M. Sherlock, D. A. Alessi, M. Bowers, B. P. Golick, M. R. Hermann, D. Kalantar, K. N. Lafortune, A. J. Mackinnon, A. Macphee, M. J. Manuel, D. Martinez, M. Mauldin, L. Pelz, M. Prantil, B. Remington, R. Sigurdsson, P. Wegner, K. Youngblood, and H. Chen, Submitted to Physical Review Letters (2020).
[37] A. P. Robinson, A. V. Arefiev, and D. Neely, Physical Review Letters **111**, 1 (2013).
[38] A. J. Kemp and S. C. Wilks, Physics of Plasmas **27**, 10.1063/5.0007159 (2020).
[39] J. Fuchs, P. Antici, E. D'Humières, E. Lefebvre, M. Borghesi, E. Brambrink, C. A. Cecchetti, M. Kaluza, V. Malka, M. Manclossi, S. Meyroneinc, P. Mora, J. Schreiber, T. Toncian, H. Pépin, and P. Audebert, Nature Physics **2**, 48 (2006).
[40] M. Martinez, W. Bang, G. Dyer, X. Wang, E. Gaul, T. Borger, M. Ringuette, M. Spinks, H. Quevedo, A. Bernstein, M. Donovan, and T. Ditmire, AIP Conference Proceedings **1507**, 874 (2012).
[41] E. Gaul, T. Toncian, M. Martinez, J. Gordon, M. Spinks, G. Dyer, N. Truong, C. Wagner, G. Tiwari, M. E. Donovan, T. Ditmire, and B. M. Hegelich, Journal of Physics: Conference Series **717**, 10.1088/1742-6596/717/1/012092 (2016).
[42] H. Hinterberger and R. Winston, Review of Scientific Instruments **37**, 1094 (1966).
[43] H. Chen, A. J. Link, R. Van Maren, P. K. Patel, R. Shepherd, S. C. Wilks, and P. Beiersdorfer, Review of Scientific Instruments **79**, 3 (2008).
[44] D. Mariscal, G. J. Williams, H. Chen, S. Ayers, N. Lemos, S. Kerr, and T. Ma, Review of Scientific Instruments **89**, 10.1063/1.5039388 (2018).
[45] A. L. Meadowcroft, C. D. Bentley, and E. N. Stott, Review of Scientific Instruments **79**, 1 (2008).
[46] T. Bonnet, M. Comet, D. Denis-Petit, F. Gobet, F. Han-

nachi, M. Tarisien, M. Versteegen, and M. M. Aléonard, Review of Scientific Instruments **84**, 10.1063/1.4826084 (2013).

[47] B. R. Maddox, H. S. Park, B. A. Remington, N. Izumi, S. Chen, C. Chen, G. Kimminau, Z. Ali, M. J. Haugh, and Q. Ma, Review of Scientific Instruments **82**, 10.1063/1.3531979 (2011).

[48] G. Jackson Williams, B. R. Maddox, H. Chen, S. Kojima, and M. Millecchia, Review of Scientific Instruments **85**, 11 (2014).

[49] M. M. Marinak, S. G. Glendinning, R. J. Wallace, B. A. Remington, K. S. Budil, S. W. Haan, R. E. Tipton, and J. D. Kilkenny, Physical Review Letters **80**, 4426 (1998).

[50] J. Ferri, E. Siminos, and T. Fülöp, Communications Physics **2**, 10.1038/s42005-019-0140-x (2019).

[51] T. D. Arber, K. Bennett, C. S. Brady, A. Lawrence-Douglas, M. G. Ramsay, N. J. Sircombe, P. Gillies, R. G. Evans, H. Schmitz, A. R. Bell, and C. P. Ridgers, Plasma Physics and Controlled Fusion **57**, 113001 (2015)
.